

Earth's Future

RESEARCH ARTICLE

10.1029/2023EF003937

Song Liu and Lei Shu contributed equally to this study.

Key Points:

- We detect enhanced SO₂ and NO₂ columns over power plants during heatwaves
- We provide evidence of increasing electricity use and emissions in the power sector
- Elevated precursor emissions facilitate PM_{2.5} and O₃ formation in an inhomogeneous manner under the combined effect of chemistry and meteorology

Supporting Information:

Supporting Information may be found in the online version of this article.

Correspondence to:

L. Zhu,
zhu13@sustech.edu.cn

Citation:

Liu, S., Shu, L., Zhu, L., Song, Y., Sun, W., Chen, Y., et al. (2024). Underappreciated emission spikes from power plants during heatwaves observed from space: Case studies in India and China. *Earth's Future*, 12, e2023EF003937. <https://doi.org/10.1029/2023EF003937>



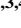

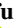




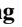


Received 10 JULY 2023
Accepted 22 JAN 2024

Author Contributions:

Conceptualization: Song Liu, Lei Shu, Lei Zhu, Yu Song
Formal analysis: Song Liu, Lei Shu, Lei Zhu
Investigation: Song Liu, Lei Shu, Lei Zhu
Methodology: Song Liu, Lei Shu, Lei Zhu, Yu Song
Supervision: Lei Zhu, Xin Yang, Tzung-May Fu
Visualization: Wenfu Sun, Yuyang Chen

© 2024 The Authors. *Earth's Future* published by Wiley Periodicals LLC on behalf of American Geophysical Union. This is an open access article under the terms of the [Creative Commons Attribution-NonCommercial-NoDerivs License](#), which permits use and distribution in any medium, provided the original work is properly cited, the use is non-commercial and no modifications or adaptations are made.

Underappreciated Emission Spikes From Power Plants During Heatwaves Observed From Space: Case Studies in India and China

Song Liu¹ , Lei Shu^{1,2} , Lei Zhu^{1,3,4} , Yu Song⁵ , Wenfu Sun^{1,6} , Yuyang Chen¹ , Dakang Wang¹, Dongchuan Pu¹, Xicheng Li¹ , Shuai Sun¹ , Juan Li¹ , Xiaoxing Zuo¹ , Weitao Fu¹, Xin Yang^{1,3,4} , and Tzung-May Fu^{1,3,4} 

¹School of Environmental Science and Engineering, Southern University of Science and Technology, Shenzhen, China, ²School of Geographical Sciences, Fujian Normal University, Fuzhou, China, ³Guangdong Provincial Observation and Research Station for Coastal Atmosphere and Climate of the Greater Bay Area, Shenzhen, China, ⁴Shenzhen Key Laboratory of Precision Measurement and Early Warning Technology for Urban Environmental Health Risks, School of Environmental Science and Engineering, Southern University of Science and Technology, Shenzhen, China, ⁵State Key Joint Laboratory of Environmental Simulation and Pollution Control, College of Environmental Sciences and Engineering, Peking University, Beijing, China, ⁶Royal Belgian Institute for Space Aeronomy (BIRA-IASB), Brussels, Belgium

Abstract The frequency, intensity, and duration of extreme heatwaves are projected to increase in the global context of climate change. However, evidence of how anthropogenic emissions respond to heatwaves and further impact air quality remains elusive. Here, we use satellite remote sensing measurements alongside chemical transport model simulations to reveal abrupt variations in primary and secondary air pollutants introduced by extreme heatwaves. We highlight evidence from China and India, where satellite sulfur dioxide (SO₂) and nitrogen dioxide (NO₂) columns over thermal power plants enhance consistently responding to heatwaves. We attribute such spiked emissions to soaring electricity use and demonstrate that bottom-up inventories underestimate the emissions from the power sector by 34.9% for the selected case. Elevated emissions facilitate fine particulate matter (PM_{2.5}) and ozone (O₃) formation over thermal power plants in an inhomogeneous manner, due to the combined effect of atmospheric oxidizing capacity, thermal decomposition of peroxyacetyl nitrate, planetary boundary layer rise, and air stagnation. Our results underscore the emerging challenge of pollution control attributable to the increasing climate penalty and the necessity of targeted control strategies and alternative energy sources during heatwaves.

Plain Language Summary Heatwaves are associated with high ambient temperatures and adverse health outcomes, but how anthropogenic emissions of atmospheric pollutants respond to heatwaves remains less explored. Here, we provide evidence from space for the first time that sulfur dioxide (SO₂) and nitrogen dioxide (NO₂) over thermal power plants enhance consistently responding to heatwaves. We attribute such spiked emissions to soaring electricity use, a feedback previously overlooked by state-of-the-art emission inventories. The enhanced emissions increase levels of fine particulate matter (PM_{2.5}) and surface ozone (O₃) in an inhomogeneous manner during heatwaves due to the combined effect of chemistry and meteorology.

1. Introduction

The increase in global surface temperature under a warmer climate is followed by a rise in frequency, intensity, and duration of summer heatwaves (IPCC, 2021). The influences of extreme heatwaves include excess mortality (Mazdiyasi et al., 2017; Yang et al., 2021), agricultural loss (Brás et al., 2021), and air quality degradation. Previous studies have suggested that heatwaves associated with stagnant meteorological conditions exacerbate urban air quality by accumulating secondary pollutants such as fine particulate matter (PM_{2.5}) and ozone (O₃) (Pyrgou et al., 2018; Schnell & Prather, 2017; Tressol et al., 2008). The synoptic meteorological pattern additionally triggers multiple feedback, including accelerated photochemical reactions (Lei et al., 2022), enhanced biogenic emissions (Churkina et al., 2017; Ma et al., 2019), reduced dry deposition by vegetation (Lin et al., 2020), and increased likelihood of wildfire risk (Libonati et al., 2022).

Aside from natural interactions, extreme heatwaves commonly introduce soaring electricity demand from residential cooling and agricultural irrigation (Auffhammer et al., 2017; Salamanca et al., 2013). In turn, the spiked generation of thermal power is accompanied by surged demand for fossil fuels and emissions of air pollution

Writing – original draft: Song Liu, Lei Shu, Lei Zhu
Writing – review & editing: Song Liu, Lei Shu, Lei Zhu, Yu Song, Wenfu Sun, Yuyang Chen, Dakang Wang, Dongchuan Pu, Xicheng Li, Shuai Sun, Juan Li, Xiaoxing Zuo, Weitao Fu, Xin Yang, Tzung-May Fu

Table 1
Observed Changes in SO₂ and NO₂ Columns Over Coal-Fired Power Plants for the 2019 Indian Heatwave and the Anthropogenic and Meteorological Contributions

(a) Observed change	SO ₂	44.3 (±8.2)%
	NO ₂	23.7 (±7.1)%
(b) Reported change from annual trend	SO ₂	4.1% (Qu et al., 2019)
	NO ₂	2.9% (Miyazaki et al., 2017)
(c) Change contributed by meteorology and chemical feedbacks	SO ₂	18.2 (±4.7)%
	NO ₂	13.2 (±5.2)%
(d) Change contributed by anthropogenic emissions		34.9%

Note. (a) TROPOMI satellite measurements averaged over thermal power plants with installed capacity greater than 1,000 MW. (b) long-term annual trends for thermal power plants from literature. (c) meteorological effects quantified using numerical simulations with the same anthropogenic emissions. (d) emission changes in the power sector constrained by reproducing emission impacts on the observed SO₂ column changes via perturbation simulations. Values in parathesis are standard errors of the means accounting for the number of days with valid data.

precursors. Sulfur dioxide (SO₂) and nitrogen oxides (NO_x = NO₂ + NO) are important primary production pollutants arising mainly from fossil fuel combustions. Human exposure to SO₂ and NO_x are associated with adverse health outcomes such as respiratory infections and asthma symptoms (Achakulwisut et al., 2019; Kobayashi et al., 2020; Pannullo et al., 2017). In addition, SO₂ and NO_x are precursors to secondary PM_{2.5} and O₃, which are recognized as threat to human health (Day et al., 2017; Xing et al., 2016) and as short-lived climate pollutants contributing to climate change (Seinfeld & Pandis, 2016). Past studies relying on ground-based data have noticed that SO₂ and NO_x emissions from thermal power plants in the United States correlate linearly with air temperature during heatwaves and consequently increase PM_{2.5} and O₃ levels (Abel et al., 2017; Farkas et al., 2015; He et al., 2013).

When sparse ground-based observations are unavailable, and uncertain bottom-up emission data are outdated, near real-time measurements from space-based platforms represent an attractive means of monitoring atmospheric pollutant abundances. Global SO₂ and NO₂ measurements have been stably provided by the Ozone Monitoring Instrument (OMI) satellite sensor since 2005 and widely used to monitor variations in fossil fuel consumption (Krotkov et al., 2016; F. Liu et al., 2020; van der A et al., 2017). Compared to its predecessor OMI, the TROPospheric Monitoring Instrument (TROPOMI) spectrometer with a finer spatial resolution (up to 5.6 km × 3.6 km) and a higher instrument sensitivity has revolutionized our capability in monitoring emissions from point sources including thermal power plants (Cooper et al., 2022; Fioletov et al., 2020; Goldberg et al., 2019; S. Liu et al., 2021; Levelt et al., 2022).

In this study, we focus on anthropogenic emission enhancements from fossil fuel combustion responding to heatwaves and their impacts on air quality. We begin by employing OMI and TROPOMI satellite measurements to monitor SO₂ and NO₂ variations over thermal power plants during heatwaves. We next apply a regional Weather Research and Forecasting model coupled with Chemistry (WRF-Chem) chemical transport model to disentangle meteorological impact on the observed changes, from which we quantify enhancements in anthropogenic emissions in the power sector. On the basis of the satellite-constrained emissions, we conclude by quantifying sensitivities of PM_{2.5} and O₃ production to growths in precursor emissions during heatwaves. Our results, for the first time, reveal the abrupt heatwave-related increases of power plant emissions using satellite observations and highlight the unperceived roles of heatwaves on the formation of secondary air pollutants.

2. Materials and Methods

2.1. Satellite SO₂ and NO₂ Observations

We use total SO₂ and tropospheric NO₂ columns from OMI and TROPOMI. The OMI instrument, launched in 2004, is an ultraviolet-visible push-broom imaging spectrometer on board the US National Aeronautics and Space Administration (NASA) Aura satellite. TROPOMI is the single payload of the European Space Agency (ESA) Sentinel-5 Precursor satellite launched in 2017, covering wavelength bands between the ultraviolet and the shortwave infrared. Both sensors provide nearly daily global observations with an overpass time of 13:30 local

time. The ground pixel sizes are approximately $13 \text{ km} \times 24 \text{ km}$ (along-track \times cross-track) for OMI and $7.2 \text{ km} \times 3.6 \text{ km}$ for TROPOMI ($5.6 \text{ km} \times 3.6 \text{ km}$ after August 2019).

We use Level 2 data of the NASA OMI V003 standard products and the ESA TROPOMI operational products (RPRO v1 for 2019 and v2 for 2022) with details summarized in Table S1 in Supporting Information S1. We remove OMI measurements with large cloud fractions and pixels affected by row anomalies. We use the quality assurance values ($qa_value > 0.75$) to select TROPOMI pixels, which correspond to data with mostly clear-sky and data meeting quality criteria (Theys et al., 2017; van Geffen et al., 2021). For SO_2 , we additionally eliminate edge pixels from the orbital swath due to the increased noise. OMI and TROPOMI NO_2 data are regridded to resolutions of $0.25^\circ \times 0.25^\circ$ and $0.1^\circ \times 0.1^\circ$, respectively, based on an area-weighted tessellation. An extended area of $0.4^\circ \times 0.4^\circ$ is adapted for SO_2 , considering its longer lifetime and higher noise than NO_2 , as recommended by Levelt et al. (2022). We exclude power plants with limited anthropogenic emissions (mean SO_2 or NO_2 columns lower than $1 \times 10^{15} \text{ molec. cm}^{-2}$) or with potential interferences from active fires (<https://www.earthdata.nasa.gov/firms>) from the analysis. For time series analysis, we compute 7-day running averages to smooth out daily fluctuations in satellite columns due to retrieval noise, including the effects of clouds and meteorology. See Text S1 in Supporting Information S1 for uncertainty discussions.

2.2. WRF-Chem Model Simulations

We run the WRF-Chem version 4.1 (Grell et al., 2005) chemical transport model to simulate air pollutant concentrations for the selected 2019 case, as summarized in Table S2 in Supporting Information S1. The meteorological initial and boundary conditions are from the National Centers for Environmental Prediction (NCEP) Final (FNL) operational global analysis with a temporal resolution of 6 hr and a spatial resolution of $0.25^\circ \times 0.25^\circ$ (<https://rda.ucar.edu/datasets/ds083.3>). The chemical initial and boundary conditions are from the Community Atmosphere Model with Chemistry (CAM-chem) simulation outputs at a $0.9^\circ \times 1.25^\circ$ horizontal resolution (Buchholz et al., 2019).

Anthropogenic emissions are from the Emissions Database for Global Atmospheric Research-Hemispheric Transport of Air Pollution inventory (Janssens-Maenhout et al., 2015) for the year of 2010 at the $0.1^\circ \times 0.1^\circ$ resolution. Biogenic emissions are calculated online using the Model of Emissions of Gases and Aerosols from Nature framework (Guenther et al., 2012). Fire emissions are from Fire INventory from NCAR (FINN) version 1.5 (Wiedinmyer et al., 2011). We select the CBMZ chemical mechanism (Zaveri & Peters, 1999) for gas-phase chemistry and the MOSAIC aerosol scheme configured with 4 sectional aerosol bins (Zaveri et al., 2008). For the simulation period (30 May–15 June), we use a spin-up time of 72 hr and a temporal resolution of 1 hr.

The simulations adopt a modeling domain centered at 22.0°N , 82.5°E (Figure S1 in Supporting Information S1), including 34 vertical layers extending from the surface to 50 hPa at a grid resolution of $10 \text{ km} \times 10 \text{ km}$. For SO_2 and NO_2 analysis, we apply the satellite averaging kernels to the modeled vertical profiles to remove errors resulting from a priori profile assumptions (Eskes & Boersma, 2003), and we sample the model outputs in space and time to the valid satellite grids. To consider the influences of year-to-year fire emissions on our $\text{PM}_{2.5}$ and O_3 analysis, two perturbation tests are achieved by employing 2018 fire emissions on 2019 simulation and vice versa (not shown). From that, cities affected by fires, mainly located in eastern India, are excluded from the analysis. See Text S2 in Supporting Information S1 for model evaluation and uncertainty discussions.

2.3. Emission Inversion

While emission constraints with inverse modeling such as the adjoint-based approach and variety of mass balance methods are potentially influenced by observational uncertainties or simplified assumptions (Cooper et al., 2017), we instead use a perturbation simulation approach with full treatment of chemistry and transport following Sun et al. (2021). Following an approximately linear response of columns to emission changes, we conduct an array of WRF-Chem perturbation simulations to reproduce the emission impacts on the observed changes in SO_2 columns. Due to the use of relative differences in describing emission impacts and observed changes, the method is less sensitive to absolute values of a priori emission inventories or model uncertainties. Here, we select SO_2 as the emission indicator because of its lower contamination from other sources, such as transportation (2.5% in comparison with 37.1% for NO_2 ; M. Li et al., 2017).

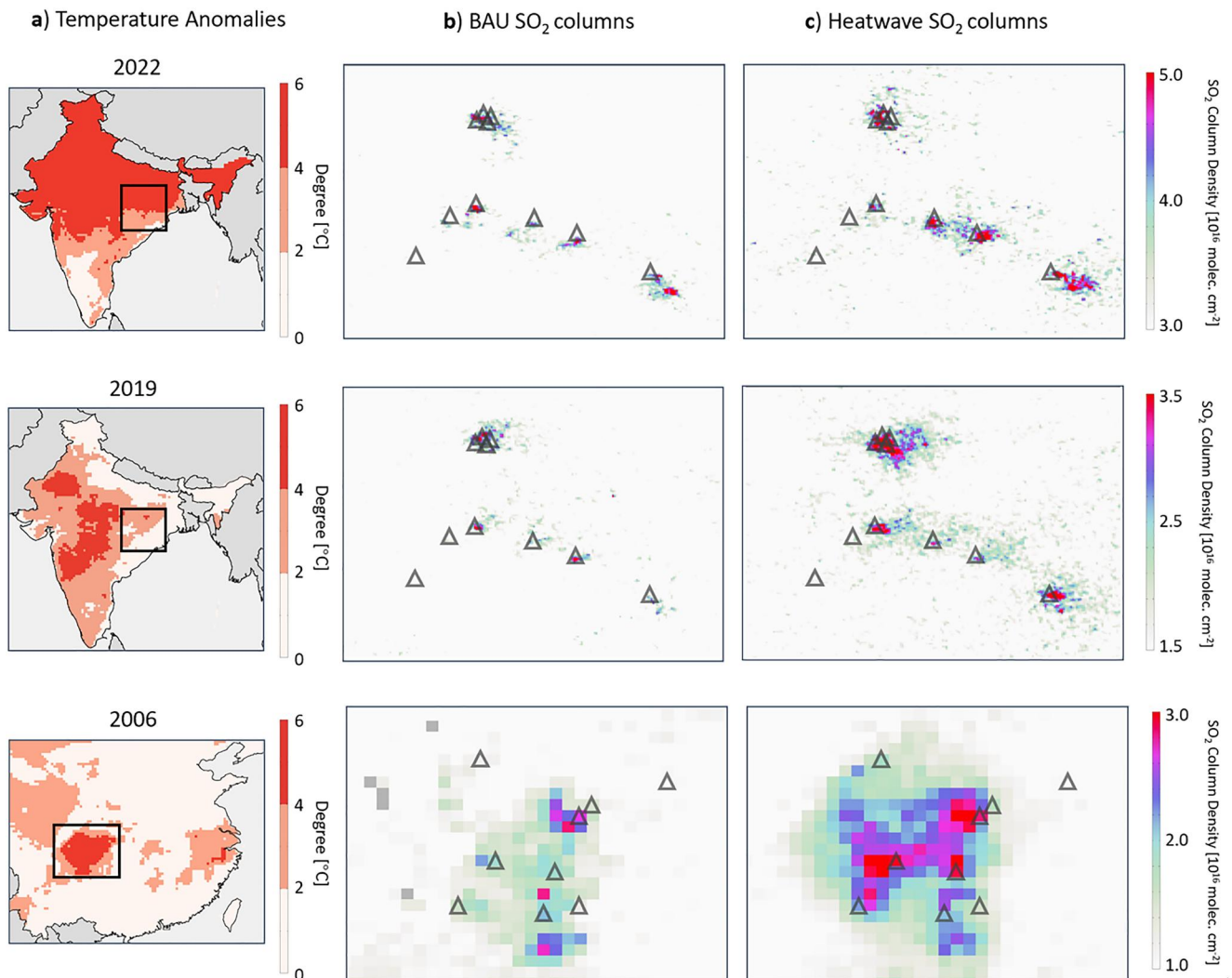


Figure 1. Satellite-observed enhancements in SO_2 columns during heatwaves. Results are shown for the heatwaves in 2022 (15 March–26 March, India), 2019 (30 May–15 June, India), and 2006 (01 August–31 August, China). Heatwave severity in panel (a) is measured as the 2-m daily maximum temperature anomalies relative to the 1981–2000 climatology, based on ERA5 reanalysis data (<https://cds.climate.copernicus.eu>). Black boxes in panel (a) show the geographic regions used in panels (b, c) with intensive power plant clusters. Total SO_2 columns observed by TROPOMI (2022 and 2019 events) and Ozone Monitoring Instrument (2006 event) are compared for heatwave conditions (c) and the same periods in previous years (b). Triangles in panels (b, c) pinpoint the top largest thermal power plants. See Figure S2 in Supporting Information S1 for difference maps.

2.4. Power Plant and City Database

Information on Chinese thermal power plants for the year 2006 is from <https://www.carbon-brief.org>. The location and generation capacity information of Indian thermal power plants are provided by the World Resources Institute (<https://datasets.wri.org>) and adjusted for year-to-year evolutions based on information from the Global Energy Monitor (<https://globalenergymonitor.org>). The location and population of Indian cities are listed at the GeoNames geographical database (<https://www.geonames.org>).

3. Results and Discussion

3.1. Elevated SO_2 and NO_2 Levels Probed From Space

Figures 1 and 2 examine the total SO_2 columns and tropospheric NO_2 columns during extreme heatwaves, where the TROPOMI and OMI satellite instruments observe consistent enhancements over regions with intensive coal-based power plants. Events are shown for the 2022 early and prolonged spring heatwave in India and three record-

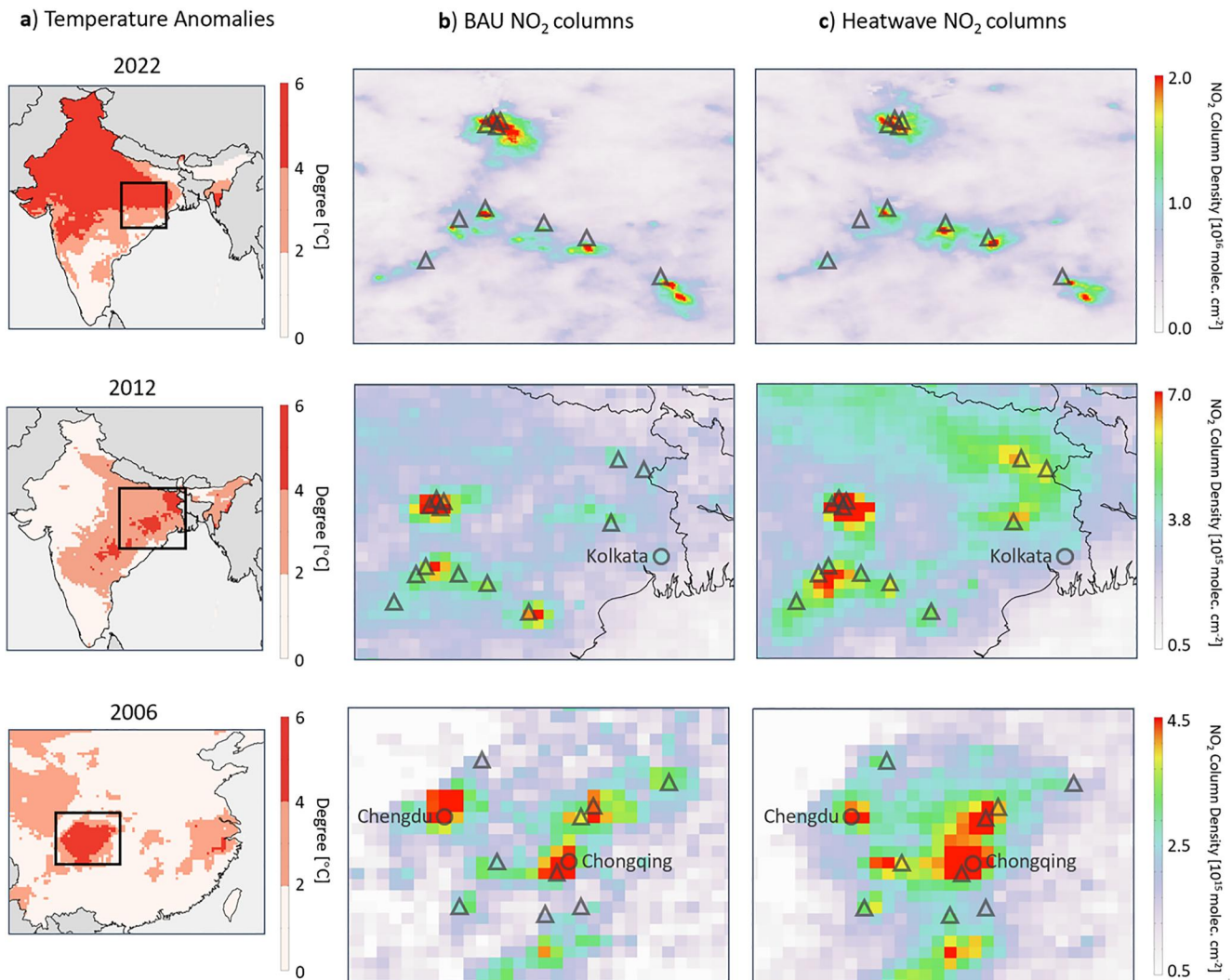


Figure 2. Similar to Figure 1 but for tropospheric NO₂ columns during heatwaves in 2022 (15 March–26 March, India), 2012 (23 May–02 June, India), and 2006 (01 August–31 August, China). Measurements provided by TROPOMI (2022 event) and Ozone Monitoring Instrument (2012 and 2006 events) are compared for heatwave conditions (c) and the same periods in previous years (b). Circles in panels (b, c) show mega cities of Kolkata (22.57°N, 88.36°E, India), Chengdu (30.66°N, 104.07°E, China), and Chongqing (29.44°N, 106.89°E, China). See Figure S3 in Supporting Information S1 for difference maps.

breaking summer heatwaves affecting densely populated regions of Asia (2019 in India, 2012 in India, and 2006 in China). Hereafter, an extreme heatwave is defined as a period of three or more consecutive days with daily maximum temperature departure from climatology higher than 6.4°C (IMD, 2018; WMO & WHO, 2015).

Inspection of the mean columns over thermal power plants reveals 26.5%–83.8% enhancements for SO₂ and 4.1%–23.7% for NO₂ during heatwaves, in comparison with the same period in the previous year (Table S3 in Supporting Information S1). Except for the 2022 spring heatwave, the reference periods in the previous years for summer heatwaves show temperatures relatively close to the multi-year climatology with average biases ranging between $-0.66 \pm 1.14^\circ\text{C}$ and $0.41 \pm 1.36^\circ\text{C}$ (Figure S4 in Supporting Information S1). The reported column enhancements exceed the long-term annual growth owing to the overall economic development (by up to 4.1% for SO₂ and 2.9% for NO₂; F. Liu et al., 2016; Miyazaki et al., 2017; Qu et al., 2019) and cannot be explained by meteorological influences alone (see next section), highlighting potential emission spikes during heatwaves. Our estimation possibly overestimates column variations for China, due to the typically higher electricity use and attributable emissions from a thermal power plant in the afternoon (overpass time of OMI and TROPOMI).

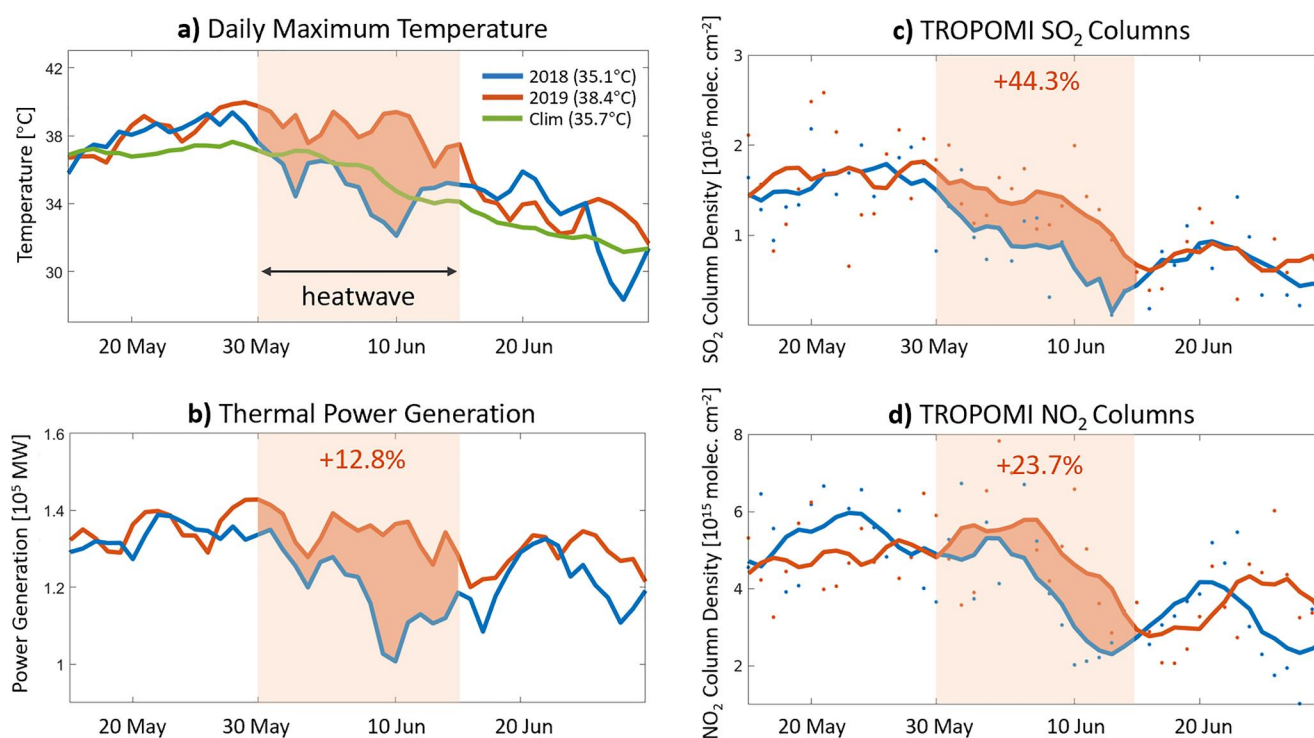


Figure 3. Dynamics of SO_2 and NO_2 columns driven by temperature and power generation for the 2019 Indian heatwave compared to 2018. (a), ERA5 2-m daily maximum temperature across India for 2018, 2019, and climatology (1980–2000; green). Average temperatures during the heatwave period are given in parentheses. (b), reported daily power generation from coal-fired power plants (<https://npp.gov.in>). (c, d), averaged SO_2 ($0.25^\circ \times 0.25^\circ$) and NO_2 ($0.1^\circ \times 0.1^\circ$) columns within TROPOMI grids for a total of 93 thermal power plants with installed capacity larger than 1,000 MW. Dots show daily averages, and solid lines in panels (c, d) represent 7-day moving averages. Mean increases for daily values during heatwave are inserted in panels (b, c, d).

However, for India with higher demand than supply for electricity, large power plants typically run at full capacity throughout the day and do not show an apparent diurnal cycle in productivity and emissions (Ghude et al., 2020). Differences between SO_2 and NO_2 results can be explained by the different species lifetime, data quality and selection criteria, as well as contamination by other emission sources (Levelt et al., 2022). In the following, we focus on the 2019 Indian heatwave, one of the most severe heatwaves regarding the severity, spatial, and temporal extent (Ray et al., 2021).

As coal source conventionally accounts for more than 70% of the total electricity production in India and China (<http://data.worldbank.org>), we attribute the observed SO_2 and NO_2 enhancements primarily to the rising electricity demand borne by coal combustion. Figure 3 presents time-series of surface temperature, thermal power generation, as well as satellite SO_2 and NO_2 columns for TROPOMI grids containing coal-fired power plants in the presence and absence of heatwave. SO_2 and NO_2 divergences between 2019 and 2018 exhibit agreements with the time-line of reported power generation from coal source. On average, heatwave-induced increase in power generation (12.8%) simultaneously introduces growths in SO_2 column (44.3%) and NO_2 column (23.7%).

Although coal combustion contributes to more than 95% of total SO_2 and NO_x emissions over thermal power plants (M. Li et al., 2018), the relationship between top-down columns and bottom-up emissions could be complicated by variable meteorology and non-linear chemical feedbacks. Figures 4 and S5 in Supporting Information S1 show the NO_2 variations captured by TROPOMI over top largest power plants during the 2019 Indian heatwave relative to the same period in 2018. TROPOMI clearly captures NO_2 enhancement plumes downwind from single or clusters of power plants responding to the extreme heatwave with potential influences from topography (e.g., for power plant 1) and urban outflow (e.g., for power plant 2). TROPOMI NO_2 variations above individual power plants vary from -27.1% to 46.1% (Table S4 in Supporting Information S1), depending on both emission strengths and meteorological conditions.

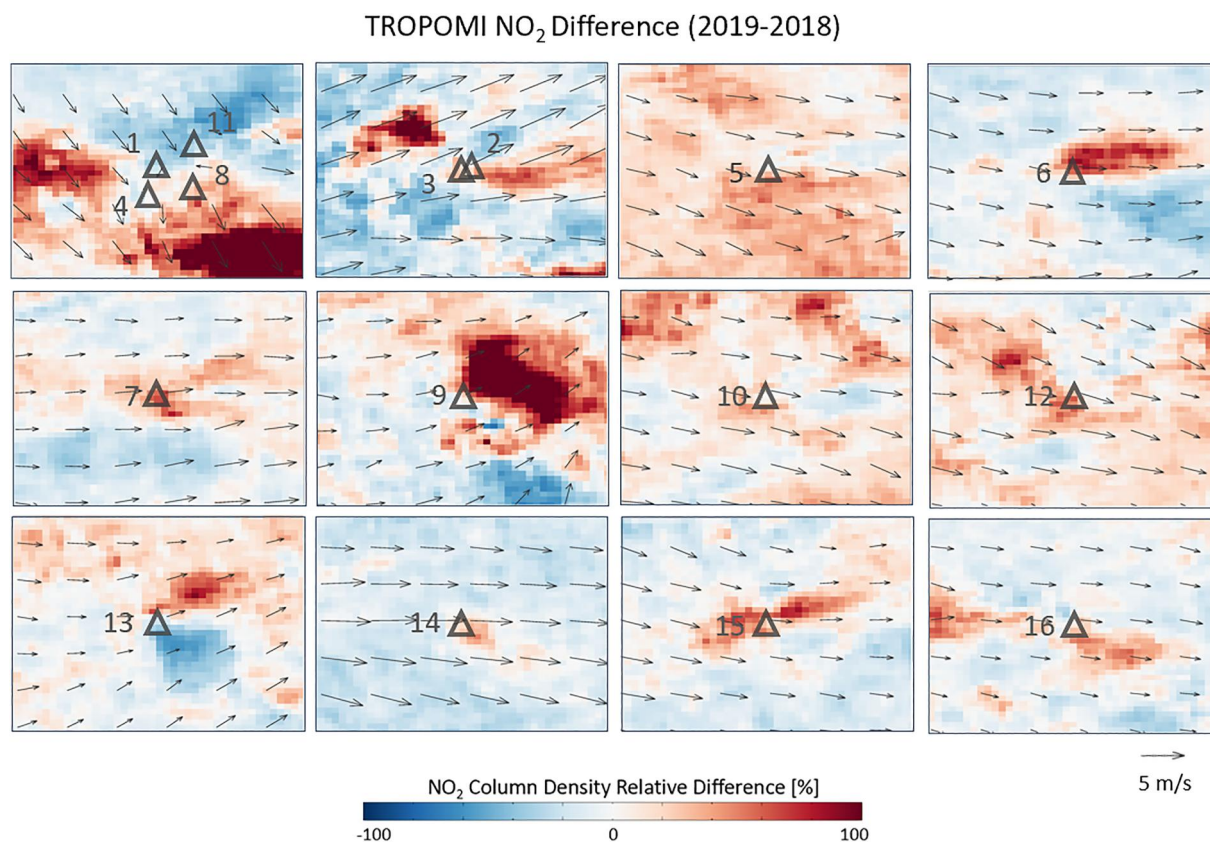


Figure 4. Relative changes in TROPOMI NO₂ columns over top power plants during the 2019 Indian heatwave relative to the same period in 2018. The power plant plots with a 1° × 1° domain are sorted with the installed power generation capacity in descending order. A regridding resolution of 0.025° × 0.025° is used for illustration purposes. Arrows show ERA5 10-m wind vectors interpolated to TROPOMI overpass time (13:30 local time). Triangles indicate power plants, with numbers indicating rankings in power generation capacity. See Table S4 in Supporting Information S1 for information about power plants.

3.2. Power Plant Emission Growths Responding to Heatwaves

To quantify meteorological impact on atmospheric chemistry and transport, we adopt the state-of-the-art WRF-Chem model with consistent anthropogenic emissions but corresponding meteorological fields during heatwaves. Heatwaves are typically under the control of a high-pressure system with large-scale subsidence, which results in clear skies and calm winds (Wu et al., 2019). Such stagnant meteorological situations favor the accumulation of air pollutants, particularly for locations with heterogeneous topography (Fioletov et al., 2022; Goldberg et al., 2020). Meanwhile, the stagnation is typically accompanied by stronger chemical loss of NO_x via nitric acid within pollution plumes over the NO_x-saturated regime (Lorente et al., 2019), and the change in lifetime affects the proportionality between NO_x emissions and NO₂ columns (Laughner & Cohen, 2019). At warm temperatures, NO_x lifetime is also affected by the thermal decomposition rate of peroxyacetyl nitrate, which becomes more rapid as temperature increases (Singh, 2015) but saturates at extremely high temperatures (above 40°C; Steiner et al. (2010)).

However, we find that the observed column growths (44.3% for SO₂ and 23.7% for NO₂ in Table 1a) are not mainly driven by meteorology and chemical feedbacks (18.2% for SO₂ and 13.2% for NO₂ in Table 1c). Here, the meteorological influences are likely dominated by wind fields, as other variables, such as temperature, boundary layer height, and sun angle, mostly reduce air pollutant concentrations during heatwaves. Upon excluding the meteorological influences and changes in chemical feedbacks (Table 1c) from the observed changes (Table 1a), we estimate that impacts from emissions on columns are 26.1% for SO₂ and 10.5% for NO₂ during the extreme heatwave. By simultaneously scaling up SO₂ and NO_x emissions in the power sector at a step of 10%, WRF-Chem reproduces the anthropogenic impact when applying an increase of 34.9% in emissions upon linear interpolation (Figure 5), with SO₂ as an emission indicator considering the low contamination from other sources.

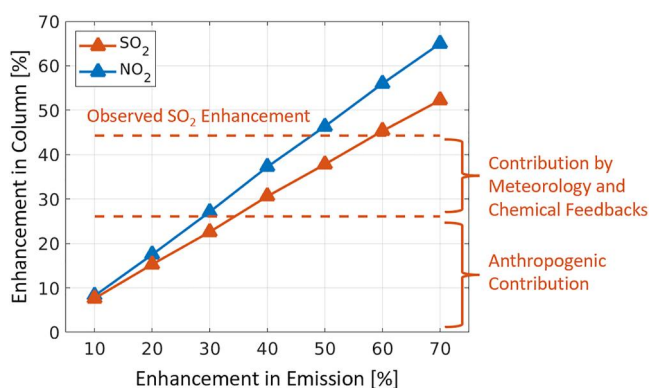


Figure 5. Response of modeled enhancements in total SO₂ and tropospheric NO₂ columns to the scaling-up of SO₂ and NO_x emissions in the power sector over thermal power plants in India during the 2019 heatwave. Results are obtained from a series of WRF-Chem perturbation simulations at a 10% step. The observed SO₂ increase (44.3%) and its meteorological contribution (18.2%) and anthropogenic contribution (26.1%) are also shown. The result takes the difference in meteorological conditions between 2018 and 2019 into consideration by running the model with corresponding meteorological fields.

3.3. Impact of Spiked Power Plant Emissions on PM_{2.5} and O₃ Formation

Our finding about spiked anthropogenic emissions during heatwaves raises the interest in assessing their role in secondary pollutant formation. With satellite-constrained emissions, we perform WRF-Chem sensitivity simulations to examine responses of surface PM_{2.5} and O₃ to the growths of SO₂ and NO_x emissions in the presence and absence of heatwaves. Figure 6 compares the daily PM_{2.5} and daily maximum 8 hr average (MDA8) O₃ responses in Indian cities under the 2019 heatwave condition and the 2018 business-as-usual condition. In both cases, the power-related SO₂ and NO_x emission enhancements broadly increase PM_{2.5} and O₃ levels by up to 5.5 μg m⁻³ and 4.1 ppbv, respectively. Spatially, the central and eastern India receive transport from intensive power plants upwind.

Focusing on areas with relatively low influences from wind fields in Figure 6a, we notice a suppression of PM_{2.5} enhancements in the 2019 heatwave scenario relative to 2018 for the National Capital Region, home to 46 million population located in the Indo-Gangetic Plain. We attribute this phenomenon partially to the limited water vapor and thus lower availability of hydroxyl radical (Figure S6a in Supporting Information S1), which dominates the atmospheric oxidizing capacity. In turn, the reduced atmospheric oxidizing capacity during heatwave decelerates the secondary formation of

PM_{2.5}. Additionally, the planetary boundary layer rises in heatwave (Figure S6b in Supporting Information S1), associated with the high-pressure synoptic pattern (Miralles et al., 2014) and favorable for the dilution of PM_{2.5}. Such variations in hydroxyl radical chemistry and planetary boundary layer meteorology during heatwaves are consistent with previous studies (Emmerson et al., 2007; Wu et al., 2019).

Responses of surface O₃ to anthropogenic emission increases, however, are inhomogeneous due to the non-linear O₃ chemistry. Specifically, O₃ concentrations over large power plants near Delhi in the National Capital Region experience decreases or less significant increases in 2018 (e.g., the National Capital Dadri Thermal Power Plant; Figure S7a in Supporting Information S1), likely determined by the locally enhanced NO_x-titration effect and consequently lessened O₃ production under the NO_x-saturated regime (Chen et al., 2020; Nelson et al., 2021). In the case of heatwave, we notice that such an O₃ suppression is distinctively strengthened with much higher negative O₃ variations observed. One possible explanation is the diminished role of NO_x sequestration by peroxyacetyl nitrates (Figure S7b in Supporting Information S1) at extremely high temperatures above 40°C (Figure S8a in Supporting Information S1), as suggested by Steiner et al., 2010. Besides, stagnation during heatwaves (Figure S8b in Supporting Information S1) may degrade O₃ production in the downwind of power plants by limiting the dispersion of precursors.

Distributions of PM_{2.5} and O₃ responses over cities in the National Capital Region and the surrounding area further reveal the statistically significant suppressions of secondary pollutant enhancements (Figures 7a and 7b). Defining a ratio to characterize pollution levels during a heatwave relative to the business-as-usual value, we obtain medians of 0.47 for PM_{2.5} and 0.75 for O₃ (Figures 7c and 7d). Our results suggest that the presence of extreme heatwaves appears to relieve urban PM_{2.5} and O₃ enhancements by -53% and -25%, respectively, temporarily buffering the degradation in air quality triggered by spiked precursor emissions over this populated area. On national level, nevertheless, the PM_{2.5} and O₃ pollution are broadly enhanced due to the increasing odd-oxygen (NO₂ + O₃) on the hot days, and the impacts from emission variations for downwind regions away from power plants will be investigated in future works, which can be complicated by long-range transport and variable gas lifetime.

4. Conclusions and Discussion

Our study assesses heatwave-related anthropogenic responses through satellite measurements alongside numerical simulations. Satellites capture enhancements of SO₂ (26.5%–83.8%) and NO₂ (4.1%–23.7%) columns over coal-based power plants during heatwaves, which are attributed to spiked electricity use. After controlling for changes in meteorological influences and chemical feedbacks, we notice increased emissions in

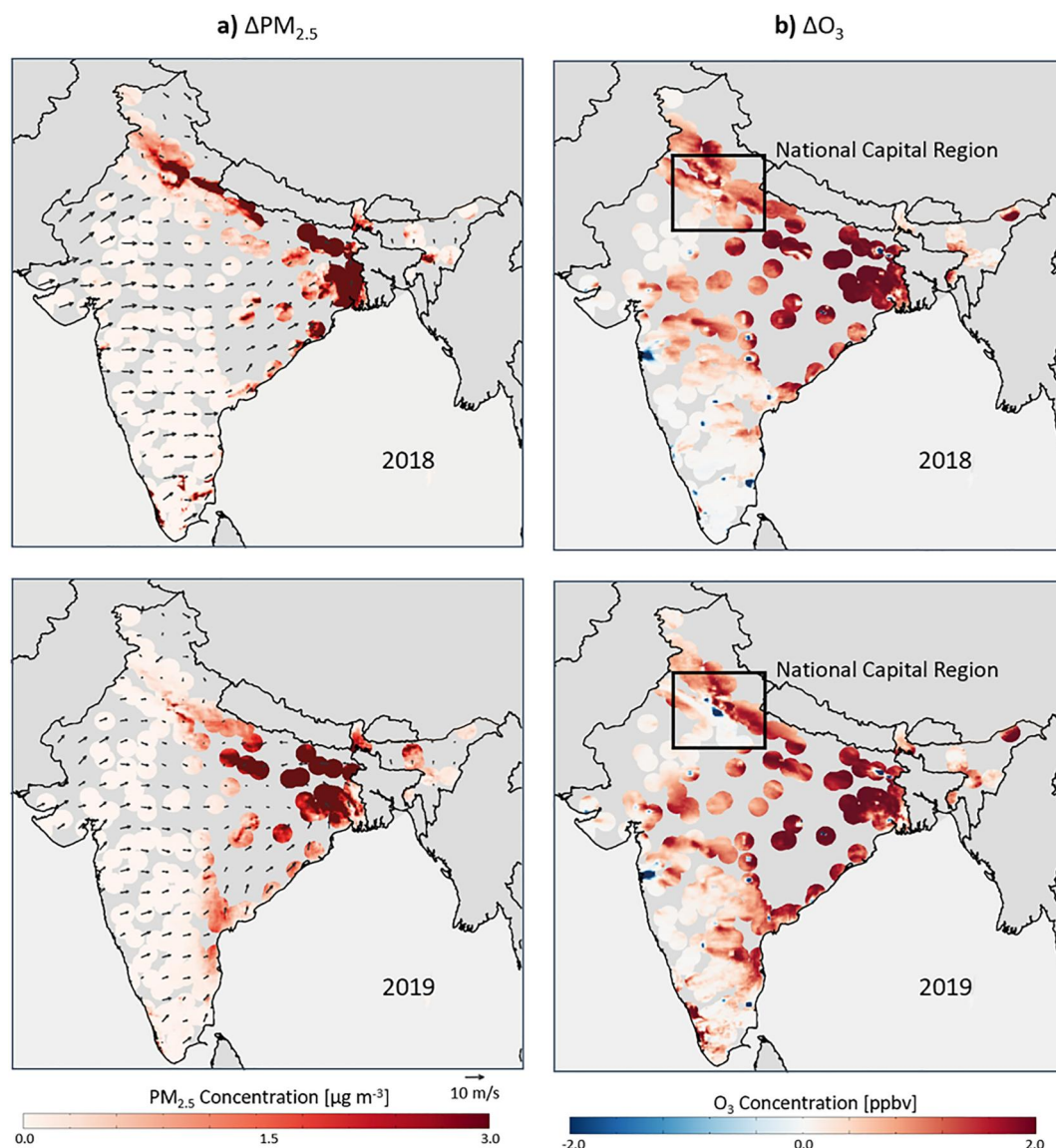


Figure 6. Daily $PM_{2.5}$ (a) and MDA8 O_3 (b) responses to the SO_2 and NO_x emission enhancements in Indian cities. Δ represent changes from the WRF-Chem base simulation to a sensitivity simulation with satellite-constraint emissions in the power sector (increase by 34.9% compared to the base simulation). Values are compared between the 2019 heatwave condition and the 2018 BAU condition. Results are shown for cities with a population greater than 100,000 and with at least a power plant within a 60 distance. 60 km is the potential influencing scope of power plants, calculated as the median distance between cities and their closest neighboring power plants across India. Arrows in panel (a) present the 10-m wind vectors. Black boxes in panel (b) locate the National Capital Region and its surround regions analyzed in Figures 7, S7, and S8 in Supporting Information S1.

the power sector by 34.9% for the selected 2019 Indian heatwave case. Our results demonstrate that daily temporal allocation of bottom-up emission inventories is important and should be implemented using surrogates that account for changes in daily temperature. Due to the lack of real-time emission measurements, current temporally resolved emission inventories are usually estimated at an annual scale and scaled to into monthly, daily, or hourly resolutions considering temporal variations in fuel consumption (Zheng et al., 2021) or electricity generation (Guevara et al., 2021). These activity indicator-based estimates might not always be able to capture the fluctuations in emissions, especially for periods with unexpected socio-economic activities.

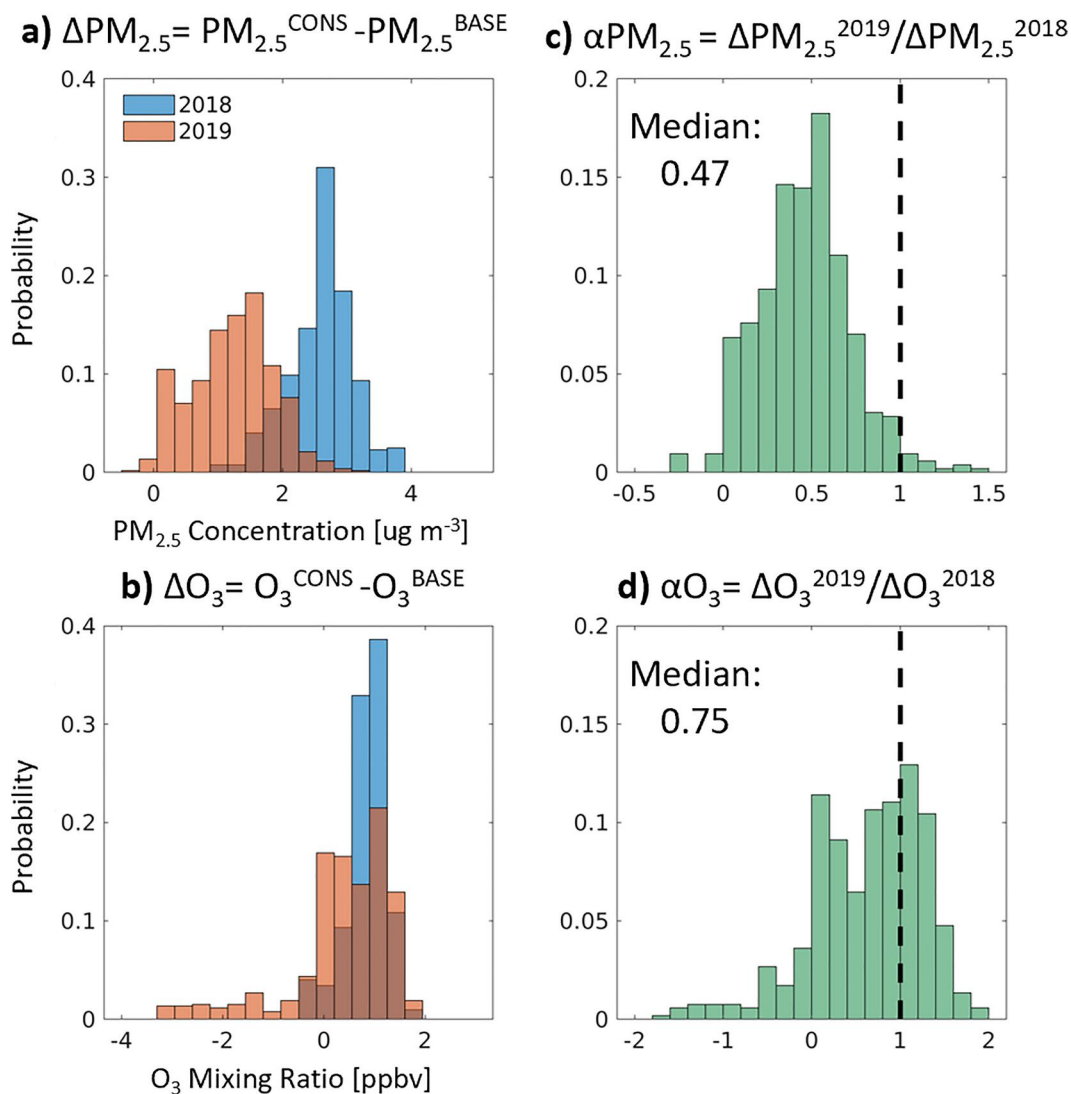


Figure 7. Sensitivities of the $PM_{2.5}$ and MDA8 O_3 to power-induced SO_2 and NO_x emission enhancements over the National Caption Region and the surrounding regions. (a, b), $\Delta PM_{2.5}$ and ΔO_3 represent changes from the WRF-Chem base simulation (BASE) to a sensitivity simulation with satellite-constraint emissions in the power sector (CONS). (c, d), $\alpha PM_{2.5}$ and αO_3 indicate ratios of $\Delta PM_{2.5}$ and ΔO_3 under the heatwave condition (2019) to the business-as-usual condition (2018), with medians inset. Results are analyzed for $40 \text{ km} \times 40 \text{ km}$ domains around city centers. The selection of 40 km compromises a sufficient number of available data points and low interference from neighboring cities for this populated region. The geographic extent of the National Caption Region and the surrounding regions are outlined in Figure 6b.

The precursor emission growths post additional challenges for $PM_{2.5}$ and O_3 pollution control (up to $5.5 \mu\text{g m}^{-3}$ and 4.1 ppbv , respectively). Moreover, we show complex influences of heatwaves on $PM_{2.5}$ and O_3 formation. Compared to non-heatwave condition, the presence of extreme heat can suppress $PM_{2.5}$ and O_3 enhancements (by -53% and -25% , respectively) from an anthropogenic perspective, under the joint influences of atmospheric oxidizing capacity, thermal decomposition of peroxyacetyl nitrate, planetary boundary layer rise, and air stagnation. This is despite the exacerbated secondary pollution from studies on natural feedback assuming constant anthropogenic sources (Schnell & Prather, 2017) and on responses of power plant emissions in the NO_x -sensitive regime (He et al., 2013). These results pinpoint the challenge of mitigating air pollution under climate change and the urgency of coordinated control policies during heatwaves.

We investigate selected high-impact heatwaves in India and China, but our results are relevant beyond these cases. Under the current changing climate, heatwaves affect 6.6% of the globe with a mean temperature of 35.6°C and a mean duration of 10.1 consecutive days, and all three metrics show rising trends (Figure S9 in Supporting Information S1) in line with regional studies (Dong et al., 2021; Hulley et al., 2020). While each heatwave is

unique regarding local meteorological conditions and energy structure, similar heatwave responsiveness to electricity demand can be expected across the globe (Auffhammer et al., 2017). Heatwaves also strongly constrain electricity generations from wind and hydropower, aggravating the burden on thermal power, especially for developing countries. Moreover, enhancements in thermal power generation and satellite-constrained emission feedback shall be regarded as lower limits of heatwave influences, considering the possible coal shortage and infrastructure failure.

Regardless, our study provides important implications for air pollution analysis that rely on chemical transport models by emphasizing the lack of real-time response of anthropogenic emissions. Our results underline anthropogenic feedback over thermal power plants to climate change and stress the necessity of a full picture of complex interplays among emission, chemistry, and meteorology for mitigating air pollution. Such analysis will benefit from geostationary satellite missions with high temporal resolutions, including Geostationary Environmental Monitoring Satellite (GEMS; J. Kim et al., 2020), Sentinel-4 (Ingmann et al., 2012), and Tropospheric Emissions: Monitoring of Pollution (TEMPO; Zoogman et al., 2017). Under the warming climate, a rapid energy transition from coal to renewable solar power offers an option to improve air quality and compensate the power demand during heatwaves, for which the resilience and flexibility against high temperature must also be considered (Feron et al., 2021).

Conflict of Interest

The authors declare no conflicts of interest relevant to this study.

Data Availability Statement

The OMI satellite data are available for SO₂ (C. Li, Krotkov, Leonard, & Joiner, 2020) and NO₂ (Krotkov et al., 2019). The operational TROPOMI data are available for SO₂ v1 (Copernicus Sentinel-5P (processed by ESA), 2018b), SO₂ v2 (Copernicus Sentinel-5P (processed by ESA), 2020), NO₂ v1 (Copernicus Sentinel-5P (processed by ESA), 2018a), and NO₂ v2 (Copernicus Sentinel-5P (processed by ESA), 2021). The reprocessed RPRO v2.3 NO₂ TROPOMI data are available via Eskes et al. (2021).

References

- Abel, D., Holloway, T., Kladar, R. M., Meier, P., Ahl, D., Harkey, M., & Patz, J. (2017). Response of power plant emissions to ambient temperature in the eastern United States. *Environmental Science & Technology*, 51(10), 5838–5846. <https://doi.org/10.1021/acs.est.6b06201>
- Achakulwisut, P., Brauer, M., Hystad, P., & Anenberg, S. C. (2019). Global, national, and urban burdens of paediatric asthma incidence attributable to ambient NO₂ pollution: Estimates from global datasets. *The Lancet Planetary Health*, 3(4), e166–e178. [https://doi.org/10.1016/s2542-5196\(19\)30046-4](https://doi.org/10.1016/s2542-5196(19)30046-4)
- Auffhammer, M., Baylis, P., & Hausman, C. H. (2017). Climate change is projected to have severe impacts on the frequency and intensity of peak electricity demand across the United States. *Proceedings of the National Academy of Sciences*, 114(8), 1886–1891. <https://doi.org/10.1073/pnas.1613193114>
- Brás, T. A., Seixas, J., Carvalhais, N., & Jägermeyr, J. (2021). Severity of drought and heatwave crop losses tripled over the last five decades in Europe. *Environmental Research Letters*, 16(6), 065012. <https://doi.org/10.1088/1748-9326/abf004>
- Buchholz, R. R., Emmons, L. K., & Tilmes, S., & The CESM2 Development Team. (2019). CESM2.1/CAM-chem instantaneous output for boundary conditions.
- Chen, Y., Wild, O., Ryan, E., Sahu, S. K., Lowe, D., Archer-Nicholls, S., et al. (2020). Mitigation of PM_{2.5} and ozone pollution in Delhi: A sensitivity study during the pre-monsoon period. *Atmospheric Chemistry and Physics*, 20(1), 499–514. <https://doi.org/10.5194/acp-20-499-2020>
- Churkina, G., Kuik, F., Bonn, B., Lauer, A., Grote, R., Tomiak, K., & Butler, T. M. (2017). Effect of VOC emissions from vegetation on air quality in Berlin during a heatwave. *Environmental Science & Technology*, 51(11), 6120–6130. <https://doi.org/10.1021/acs.est.6b06514>
- Cooper, M., Martin, R. V., Hammer, M. S., Levelt, P. F., Veeckind, P., Lamsal, L. N., et al. (2022). Global fine-scale changes in ambient NO₂ during COVID-19 lockdowns. *Nature*, 601(7893), 380–387. <https://doi.org/10.1038/s41586-021-04229-0>
- Cooper, M., Martin, R. V., Padmanabhan, A., & Henze, D. K. (2017). Comparing mass balance and adjoint methods for inverse modeling of nitrogen dioxide columns for global nitrogen oxide emissions. *Journal of Geophysical Research: Atmospheres*, 122(8), 4718–4734. <https://doi.org/10.1002/2016jd025985>
- Copernicus Sentinel-5P (processed by ESA). (2018a). TROPOMI Level 2 v1 NO₂ data [Dataset]. European Space Agency. <https://doi.org/10.5270/SSP-s4ljg54>
- Copernicus Sentinel-5P (processed by ESA). (2018b). TROPOMI Level 2 v1 SO₂ data [Dataset]. European Space Agency. <https://doi.org/10.5270/SSP-yr8kdpp>
- Copernicus Sentinel-5P (processed by ESA). (2020). TROPOMI Level 2 v2 SO₂ data [Dataset]. European Space Agency. <https://doi.org/10.5270/SSP-74eidii>
- Copernicus Sentinel-5P (processed by ESA). (2021). TROPOMI Level 2 v2 NO₂ data [Dataset]. European Space Agency. <https://doi.org/10.5270/SSP-9bnp8q8>
- Day, D. B., Xiang, J., Mo, J., Li, F., Chung, M., Gong, J., et al. (2017). Association of ozone exposure with cardiorespiratory pathophysiologic mechanisms in healthy adults. *JAMA Internal Medicine*, 177(9), 1344–1353. <https://doi.org/10.1001/jamainternmed.2017.2842>

Acknowledgments

This work is funded by the National Natural Science Foundation for Young Scientists of China (42205134), the Shenzhen Key Laboratory of Precision Measurement and Early Warning Technology for Urban Environmental Health Risks (ZDSYS20220606100604008), Guangdong Basic and Applied Basic Research Foundation (2021A1515110713), Guangdong University Research Project Science Team (2021KCXTD004), Major Talent Project of Guangdong Province (2021QN020924), and Shenzhen Science and Technology Program (KQTD20210811090048025, JCYJ20210324104604012, JCYJ20220530115404009). This work is supported by the Center for Computational Science and Engineering at Southern University of Science and Technology.

- Dong, Z., Wang, L., Sun, Y., Hu, T., Limsakul, A., Singhruck, P., & Pimonsree, S. (2021). Heatwaves in Southeast Asia and their changes in a warmer world. *Earth's Future*, 9(7), e2021EF001992. <https://doi.org/10.1029/2021ef001992>
- Emmerson, K. M., Carslaw, N., Carslaw, D. C., Lee, J. D., McFiggans, G., Bloss, W. J., et al. (2007). Free radical modelling studies during the UK TORCH Campaign in Summer 2003. *Atmospheric Chemistry and Physics*, 7(1), 167–181. <https://doi.org/10.5194/acp-7-167-2007>
- Eskes, H., & Boersma, K. (2003). Averaging kernels for DOAS total-column satellite retrievals. *Atmospheric Chemistry and Physics*, 3(5), 1285–1291. <https://doi.org/10.5194/acp-3-1285-2003>
- Eskes, H., van Geffen, J., Sneep, M., Veeffkind, P., Niemeijer, S., & Zehner, C. (2021). TROPOMI Level 2 RPRO v2.3 NO₂ data [Dataset]. S5P-PAL Data Portal. <https://data-portal.s5p-pal.com/products/no2.html>
- Farkas, C. M., Moeller, M. D., Felder, F. A., Baker, K. R., Rodgers, M., & Carlton, A. G. (2015). Temporalization of peak electric generation particulate matter emissions during high energy demand days. *Environmental Science & Technology*, 49(7), 4696–4704. <https://doi.org/10.1021/es5050248>
- Feron, S., Cordero, R. R., Damiani, A., & Jackson, R. B. (2021). Climate change extremes and photovoltaic power output. *Nature Sustainability*, 4(3), 270–276. <https://doi.org/10.1038/s41893-020-00643-w>
- Fioletov, V., McLinden, C. A., Griffin, D., Krotkov, N., Liu, F., & Eskes, H. (2022). Quantifying urban, industrial, and background changes in NO₂ during the COVID-19 lockdown period based on TROPOMI satellite observations. *Atmospheric Chemistry and Physics*, 22(6), 4201–4236. <https://doi.org/10.5194/acp-22-4201-2022>
- Fioletov, V., McLinden, C. A., Griffin, D., Theys, N., Loyola, D. G., Hedelt, P., et al. (2020). Anthropogenic and volcanic point source SO₂ emissions derived from TROPOMI on board Sentinel-5 Precursor: First results. *Atmospheric Chemistry and Physics*, 20(9), 5591–5607. <https://doi.org/10.5194/acp-20-5591-2020>
- Ghude, S. D., Karumuri, R. K., Jena, C., Kulkarni, R., Pfister, G., Sajjan, V. S., et al. (2020). What is driving the diurnal variation in tropospheric NO₂ columns over a cluster of high emission thermal power plants in India? *Atmospheric Environment X*, 5, 100058. <https://doi.org/10.1016/j.aeaoa.2019.100058>
- Goldberg, D. L., Anenberg, S. C., Griffin, D., McLinden, C. A., Lu, Z., & Streets, D. G. (2020). Disentangling the impact of the COVID-19 lockdowns on urban NO₂ from natural variability. *Geophysical Research Letters*, 47(17), e2020GL089269. <https://doi.org/10.1029/2020gl089269>
- Goldberg, D. L., Lu, Z., Streets, D. G., de Foy, B., Griffin, D., McLinden, C. A., et al. (2019). Enhanced capabilities of TROPOMI NO₂: Estimating NO_x from North American cities and power plants. *Environmental Science & Technology*, 53(21), 12594–12601. <https://doi.org/10.1021/acs.est.9b04488>
- Grell, G. A., Peckham, S. E., Schmitz, R., McKeen, S. A., Frost, G., Skamarock, W. C., & Eder, B. (2005). Fully coupled “online” chemistry within the WRF model. *Atmospheric Environment*, 39(37), 6957–6975. <https://doi.org/10.1016/j.atmosenv.2005.04.027>
- Guenther, A., Jiang, X., Heald, C. L., Sakulyanontvittaya, T., Duhl, T., Emmons, L., & Wang, X. (2012). The Model of Emissions of Gases and Aerosols from Nature version 2.1 (MEGAN2.1): An extended and updated framework for modeling biogenic emissions. *Geoscientific Model Development*, 5(6), 1471–1492. <https://doi.org/10.5194/gmd-5-1471-2012>
- Guevara, M., Jorba, O., Tena, C., Denier van der Gon, H., Kuenen, J., Elguindi, N., et al. (2021). Copernicus Atmosphere monitoring service TEMPO profiles (CAMS-TEMPO): Global and European emission temporal profile maps for atmospheric chemistry modelling. *Earth System Science Data*, 13(2), 367–404. <https://doi.org/10.5194/essd-13-367-2021>
- He, H., Hembeck, L., Hosley, K. M., Canty, T. P., Salawitch, R. J., & Dickerson, R. R. (2013). High ozone concentrations on hot days: The role of electric power demand and NO_x emissions. *Geophysical Research Letters*, 40(19), 5291–5294. <https://doi.org/10.1002/grl.50967>
- Hulley, G. C., Dousset, B., & Kahn, B. H. (2020). Rising trends in heatwave metrics across southern California. *Earth's Future*, 8(7), e2020EF001480. <https://doi.org/10.1029/2020ef001480>
- IMD. (2018). *Heatwave criteria, Climate Research and Services (CR & S) statement on climate of India during 2016 (Tech. Rep.)*. India Meteorological Department (IMD), Earth System Science Organization (ESSO). Ministry of Earth Sciences (MoES).
- Ingmann, P., Veihelmann, B., Langen, J., Lamarre, D., Stark, H., & Courrèges-Lacoste, G. B. (2012). Requirements for the GMES Atmosphere Service and ESA's implementation concept: Sentinels-4/-5 and-5p. *Remote Sensing of Environment*, 120, 58–69. <https://doi.org/10.1016/j.rse.2012.01.023>
- IPCC. (2021). In V. P. Zhai, A. Pirani, S. L. Connors, C. Péan, S. Berger, et al. (Eds.), *Climate Change 2021: The physical science basis. Contribution of working Group I to the Sixth assessment report of the intergovernmental panel on climate change (Tech. Rep.)*. Masson-Delmotte. Cambridge University Press. <https://doi.org/10.1017/9781009157896>
- Janssens-Maenhout, G., Crippa, M., Guizzardi, D., Dentener, F., Muntean, M., Pouliot, G., et al. (2015). HTAP_v2.2: A mosaic of regional and global emission grid maps for 2008 and 2010 to study hemispheric transport of air pollution. *Atmospheric Chemistry and Physics*, 15(19), 11411–11432. <https://doi.org/10.5194/acp-15-11411-2015>
- Kim, J., Jeong, U., Ahn, M.-H., Kim, J. H., Park, R. J., Lee, H., et al. (2020). New era of air quality monitoring from space: Geostationary Environment Monitoring Spectrometer (GEMS). *Bulletin of the American Meteorological Society*, 101(1), E1–E22. <https://doi.org/10.1175/bams-d-18-0013.1>
- Kobayashi, Y., Santos, J. M., Mill, J. G., Reis Junior, N. C., Andreão, W. L., de A. Albuquerque, T. T., & Stuetz, R. M. (2020). Mortality risks due to long-term ambient sulphur dioxide exposure: Large variability of relative risk in the literature. *Environmental Science and Pollution Research*, 27(29), 35908–35917. <https://doi.org/10.1007/s11356-020-07867-5>
- Krotkov, N. A., Lamsal, L. N., Celarier, E. A., Swartz, W. H., Marchenko, S. V., Bucsel, E. J., et al. (2017). The version 3 OMI NO₂ standard product. *Atmospheric Measurement Techniques*, 10(9), 3133–3149. <https://doi.org/10.5194/amt-10-3133-2017>
- Krotkov, N. A., Lamsal, L. N., Marchenko, S. V., Bucsel, E. J., Swartz, W. H., & Joiner, J. (2019). OMI Level 2 V003 NO₂ data [Dataset]. GES DISC. <https://doi.org/10.5067/Aura/OMI/DATA2017>
- Krotkov, N. A., McLinden, C. A., Li, C., Lamsal, L. N., Celarier, E. A., Marchenko, S. V., et al. (2016). Aura OMI observations of regional SO₂ and NO₂ pollution changes from 2005 to 2015. *Atmospheric Chemistry and Physics*, 16(7), 4605–4629. <https://doi.org/10.5194/acp-16-4605-2016>
- Laughner, J. L., & Cohen, R. C. (2019). Direct observation of changing NO_x lifetime in North American cities. *Science*, 366(6466), 723–727. <https://doi.org/10.1126/science.aax6832>
- Lei, Y., Yue, X., Liao, H., Zhang, L., Zhou, H., Tian, C., et al. (2022). Global perspective of drought impacts on ozone pollution Episodes. *Environmental Science & Technology*, 56(7), 3932–3940. <https://doi.org/10.1021/acs.est.1c07260>
- Levelt, P. F., Stein Zweers, D. C., Aben, I., Bauwens, M., Borsdorff, T., De Smedt, I., et al. (2022). Air quality impacts of COVID-19 lockdown measures detected from space using high spatial resolution observations of multiple trace gases from Sentinel-5P/TROPOMI. *Atmospheric Chemistry and Physics*, 22(15), 10319–10351. <https://doi.org/10.5194/acp-22-10319-2022>

- Li, C., Krotkov, N. A., Leonard, P., & Joiner, J. (2020). OMI Level 2 V003 SO₂ data [Dataset]. GES DISC. <https://doi.org/10.5067/Aura/OMI/202022>
- Li, M., Klimont, Z., Zhang, Q., Martin, R. V., Zheng, B., Heyes, C., et al. (2018). Comparison and evaluation of anthropogenic emissions of SO₂ and NO_x over China. *Atmospheric Chemistry and Physics*, 18(5), 3433–3456. <https://doi.org/10.5194/acp-18-3433-2018>
- Li, M., Zhang, Q., Kurokawa, J.-I., Woo, J.-H., He, K., Lu, Z., et al. (2017). MIX: A mosaic Asian anthropogenic emission inventory under the international collaboration framework of the MICS-Asia and HTAP. *Atmospheric Chemistry and Physics*, 17(2), 935–963. <https://doi.org/10.5194/acp-17-935-2017>
- Libonati, R., Geirinhas, J. L., Silva, P. S., Russo, A., Rodrigues, J. A., Belém, L. B., et al. (2022). Assessing the role of compound drought and heatwave events on unprecedented 2020 wildfires in the Pantanal. *Environmental Research Letters*, 17(1), 015005. <https://doi.org/10.1088/1748-9326/ac462e>
- Lin, M., Horowitz, L. W., Xie, Y., Paulot, F., Malyshev, S., Shevliakova, E., et al. (2020). Vegetation feedbacks during drought exacerbate ozone air pollution extremes in Europe. *Nature Climate Change*, 10(5), 444–451. <https://doi.org/10.1038/s41558-020-0743-y>
- Liu, F., Beirle, S., Zhang, Q., Dörner, S., He, K., & Wagner, T. (2016). NO_x lifetimes and emissions of cities and power plants in polluted background estimated by satellite observations. *Atmospheric Chemistry and Physics*, 16(8), 5283–5298. <https://doi.org/10.5194/acp-16-5283-2016>
- Liu, F., Page, A., Strode, S. A., Yoshida, Y., Choi, S., Zheng, B., et al. (2020). Abrupt decline in tropospheric nitrogen dioxide over China after the outbreak of COVID-19. *Science Advances*, 6(28), eabc2992. <https://doi.org/10.1126/sciadv.abc2992>
- Liu, S., Valks, P., Beirle, S., & Loyola, D. G. (2021). Nitrogen dioxide decline and rebound observed by GOME-2 and TROPOMI during COVID-19 pandemic. *Air Quality, Atmosphere & Health*, 14(11), 1737–1755. <https://doi.org/10.1007/s11869-021-01046-2>
- Lorente, A., Boersma, K., Eskes, H., Veeckind, J., Van Geffen, J., De Zeeuw, M., et al. (2019). Quantification of nitrogen oxides emissions from build-up of pollution over Paris with TROPOMI. *Scientific Reports*, 9(1), 20033. <https://doi.org/10.1038/s41598-019-56428-5>
- Ma, M., Gao, Y., Wang, Y., Zhang, S., Leung, L. R., Liu, C., et al. (2019). Substantial ozone enhancement over the North China Plain from increased biogenic emissions due to heat waves and land cover in summer 2017. *Atmospheric Chemistry and Physics*, 19(19), 12195–12207. <https://doi.org/10.5194/acp-19-12195-2019>
- Mazdiyasi, O., AghaKouchak, A., Davis, S. J., Madadgar, S., Mehran, A., Ragno, E., et al. (2017). Increasing probability of mortality during Indian heat waves. *Science Advances*, 3(6), e1700066. <https://doi.org/10.1126/sciadv.1700066>
- Miralles, D. G., Teuling, A. J., Van Heerwaarden, C. C., & Vilà-Guerau de Arellano, J. (2014). Mega-heatwave temperatures due to combined soil desiccation and atmospheric heat accumulation. *Nature Geoscience*, 7(5), 345–349. <https://doi.org/10.1038/ngeo2141>
- Miyazaki, K., Eskes, H., Sudo, K., Boersma, K. F., Bowman, K., & Kanaya, Y. (2017). Decadal changes in global surface NO_x emissions from multi-constituent satellite data assimilation. *Atmospheric Chemistry and Physics*, 17(2), 807–837. <https://doi.org/10.5194/acp-17-807-2017>
- Nelson, B. S., Stewart, G. J., Drysdale, W. S., Newland, M. J., Vaughan, A. R., Dunmore, R. E., et al. (2021). In situ ozone production is highly sensitive to volatile organic compounds in Delhi, India. *Atmospheric Chemistry and Physics*, 21(17), 13609–13630. <https://doi.org/10.5194/acp-21-13609-2021>
- Pannullo, F., Lee, D., Neal, L., Dalvi, M., Agnew, P., O'Connor, F. M., et al. (2017). Quantifying the impact of current and future concentrations of air pollutants on respiratory disease risk in England. *Environmental Health*, 16(1), 1–14. <https://doi.org/10.1186/s12940-017-0237-1>
- Pyrgou, A., Hadjinicolaou, P., & Santamouris, M. (2018). Enhanced near-surface ozone under heatwave conditions in a Mediterranean island. *Scientific Reports*, 8(1), 1–10. <https://doi.org/10.1038/s41598-018-27590-z>
- Qu, Z., Henze, D. K., Li, C., Theys, N., Wang, Y., Wang, J., et al. (2019). SO₂ emission estimates using OMI SO₂ retrievals for 2005–2017. *Journal of Geophysical Research: Atmospheres*, 124(14), 8336–8359. <https://doi.org/10.1029/2019jd030243>
- Ray, K., Giri, R., Ray, S., Dimri, A., & Rajeevan, M. (2021). An assessment of long-term changes in mortalities due to extreme weather events in India: A study of 50 years' data, 1970–2019. *Weather and Climate Extremes*, 32, 100315. <https://doi.org/10.1016/j.wace.2021.100315>
- Salamanca, F., Georgescu, M., Mahalov, A., Moustouli, M., Wang, M., & Svoma, B. (2013). Assessing summertime urban air conditioning consumption in a semiarid environment. *Environmental Research Letters*, 8(3), 034022. <https://doi.org/10.1088/1748-9326/8/3/034022>
- Schnell, J. L., & Prather, M. J. (2017). Co-occurrence of extremes in surface ozone, particulate matter, and temperature over eastern North America. *Proceedings of the National Academy of Sciences*, 114(11), 2854–2859. <https://doi.org/10.1073/pnas.1614453114>
- Seinfeld, J. H., & Pandis, S. N. (2016). *Atmospheric chemistry and physics: From air pollution to climate change*. John Wiley & Sons.
- Singh, H. (2015). Tropospheric chemistry and composition—Peroxyacetyl nitrate. In G. R. North, J. Pyle, & F. Zhang (Eds.), *Encyclopedia of atmospheric sciences* (2nd ed., pp. 251–254). Academic Press. <https://doi.org/10.1016/B978-0-12-382225-3.00433-3>
- Steiner, A. L., Davis, A. J., Sillman, S., Owen, R. C., Michalak, A. M., & Fiore, A. M. (2010). Observed suppression of ozone formation at extremely high temperatures due to chemical and biophysical feedbacks. *Proceedings of the National Academy of Sciences*, 107(46), 19685–19690. <https://doi.org/10.1073/pnas.1008336107>
- Sun, W., Zhu, L., De Smedt, I., Bai, B., Pu, D., Chen, Y., et al. (2021). Global significant changes in formaldehyde (HCHO) columns observed from space at the early stage of the COVID-19 pandemic. *Geophysical Research Letters*, 48(4), 2e020GL091265. <https://doi.org/10.1029/2020g1091265>
- Theys, N., De Smedt, I., Yu, H., Danckaert, T., van Gent, J., Hörmann, C., et al. (2017). Sulfur dioxide retrievals from TROPOMI onboard Sentinel-5 precursor: Algorithm theoretical basis. *Atmospheric Measurement Techniques*, 10(1), 119–153. <https://doi.org/10.5194/amt-10-119-2017>
- Tressol, M., Ordonez, C., Zbinden, R., Brioude, J., Thouret, V., Mari, C., et al. (2008). Air pollution during the 2003 European heat wave as seen by MOZAIC airliners. *Atmospheric Chemistry and Physics*, 8(8), 2133–2150. <https://doi.org/10.5194/acp-8-2133-2008>
- van der, A. R. J., Mijling, B., Ding, J., Koukouli, M. E., Liu, F., Li, Q., et al. (2017). Cleaning up the air: Effectiveness of air quality policy for SO₂ and NO_x emissions in China. *Atmospheric Chemistry and Physics*, 17(3), 1775–1789. <https://doi.org/10.5194/acp-17-1775-2017>
- van Geffen, J., Boersma, K. F., Eskes, H., Maasakkers, J. D., & Veeckind, J. P. (2021). TROPOMI ATBD of the total and tropospheric NO₂ data products (Tech. Rep.). SSP-KNMI-L2-0005-RP issue 2.2.0.
- Wiedinmyer, C., Akagi, S., Yokelson, R. J., Emmons, L., Al-Saadi, J., Orlando, J., & Soja, A. (2011). The fire INventory from NCAR (FINN): A high resolution global model to estimate the emissions from open burning. *Geoscientific Model Development*, 4(3), 625–641. <https://doi.org/10.5194/gmd-4-625-2011>
- WMO, & WHO. (2015). *Heatwaves and health: Guidance on warning-system development (Tech. Rep.)*. World Meteorological Organization and World Health Organization. WMO-No. 1142.
- Wu, Y., Zhao, K., Huang, J., Arend, M., Gross, B., & Moshary, F. (2019). Observation of heat wave effects on the urban air quality and PBL in New York City area. *Atmospheric Environment*, 218, 117024. <https://doi.org/10.1016/j.atmosenv.2019.117024>
- Xing, Y.-F., Xu, Y.-H., Shi, M.-H., & Lian, Y.-X. (2016). The impact of PM_{2.5} on the human respiratory system. *Journal of Thoracic Disease*, 8(1), E69.

- Yang, J., Zhou, M., Ren, Z., Li, M., Wang, B., Liu, D. L., et al. (2021). Projecting heat-related excess mortality under climate change scenarios in China. *Nature Communications*, *12*(1), 1039. <https://doi.org/10.1038/s41467-021-21305-1>
- Zaveri, R. A., Easter, R. C., Fast, J. D., & Peters, L. K. (2008). Model for simulating aerosol interactions and chemistry (MOSAIC). *Journal of Geophysical Research*, *113*(D13). <https://doi.org/10.1029/2007jd008782>
- Zaveri, R. A., & Peters, L. K. (1999). A new lumped structure photochemical mechanism for large-scale applications. *Journal of Geophysical Research*, *104*(D23), 30387–30415. <https://doi.org/10.1029/1999jd000876>
- Zheng, B., Zhang, Q., Geng, G., Chen, C., Shi, Q., Cui, M., et al. (2021). Changes in China's anthropogenic emissions and air quality during the COVID-19 pandemic in 2020. *Earth System Science Data*, *13*(6), 2895–2907. <https://doi.org/10.5194/essd-13-2895-2021>
- Zoogman, P., Liu, X., Suleiman, R., Pennington, W., Flittner, D., Al-Saadi, J., et al. (2017). Tropospheric emissions: Monitoring of pollution (TEMPO). *Journal of Quantitative Spectroscopy and Radiative Transfer*, *186*, 17–39. <https://doi.org/10.1016/j.jqsrt.2016.05.008>

References From the Supporting Information

- Chan, K. L., Wiegner, M., van Geffen, J., De Smedt, I., Alberti, C., Cheng, Z., et al. (2020). MAX-DOAS measurements of tropospheric NO₂ and HCHO in Munich and the comparison to OMI and TROPOMI satellite observations. *Atmospheric Measurement Techniques*, *13*(8), 4499–4520. <https://doi.org/10.5194/amt-13-4499-2020>
- Choi, S., Lamsal, L. N., Follette-Cook, M., Joiner, J., Krotkov, N. A., Swartz, W. H., et al. (2020). Assessment of NO₂ observations during DISCOVER-AQ and KORUS-AQ field campaigns. *Atmospheric Measurement Techniques*, *13*(5), 2523–2546. <https://doi.org/10.5194/amt-13-2523-2020>
- Gupta, M., & Mohan, M. (2015). Validation of WRF/Chem model and sensitivity of chemical mechanisms to ozone simulation over megacity Delhi. *Atmospheric Environment*, *122*, 220–229. <https://doi.org/10.1016/j.atmosenv.2015.09.039>
- Han, H., Liu, J., Shu, L., Wang, T., & Yuan, H. (2020). Local and synoptic meteorological influences on daily variability in summertime surface ozone in eastern China. *Atmospheric Chemistry and Physics*, *20*(1), 203–222. <https://doi.org/10.5194/acp-20-203-2020>
- Horton, D. E., Harshvardhan, & Diffenbaugh, N. S. (2012). Response of air stagnation frequency to anthropogenically enhanced radiative forcing. *Environmental Research Letters*, *7*(4), 044034. <https://doi.org/10.1088/1748-9326/7/4/044034>
- Inness, A., Ades, M., Agustí-Panareda, A., Barré, J., Benedictow, A., Blechschmidt, A.-M., et al. (2019). The CAMS reanalysis of atmospheric composition. *Atmospheric Chemistry and Physics*, *19*(6), 3515–3556. <https://doi.org/10.5194/acp-19-3515-2019>
- Jat, R., Gurjar, B. R., & Lowe, D. (2021). Regional pollution loading in winter months over India using high resolution WRF-Chem simulation. *Atmospheric Research*, *249*, 105326. <https://doi.org/10.1016/j.atmosres.2020.105326>
- Kim, M.-H., Yeo, H., Park, S., Park, D.-H., Omar, A., Nishizawa, T., et al. (2021). Assessing CALIOP-derived planetary boundary layer height using ground-based lidar. *Remote Sensing*, *13*(8), 1496. <https://doi.org/10.3390/rs13081496>
- Krishna, R. K., Ghude, S. D., Kumar, R., Beig, G., Kulkarni, R., Nivdange, S., & Chate, D. (2019). Surface PM_{2.5} estimate using satellite-derived aerosol optical depth over India. *Aerosol and Air Quality Research*, *19*(1), 25–37. <https://doi.org/10.4209/aaqr.2017.12.0568>
- Lamsal, L. N., Krotkov, N. A., Vasilkov, A., Marchenko, S., Qin, W., Yang, E.-S., et al. (2021). Ozone Monitoring Instrument (OMI) Aura nitrogen dioxide standard product version 4.0 with improved surface and cloud treatments. *Atmospheric Measurement Techniques*, *14*(1), 455–479. <https://doi.org/10.5194/amt-14-455-2021>
- Li, C., Krotkov, N. A., Leonard, P. J., Carn, S., Joiner, J., Spurr, R. J., & Vasilkov, A. (2020). Version 2 ozone monitoring instrument SO₂ product (OMSO2 V2): New anthropogenic SO₂ vertical column density dataset. *Atmospheric Measurement Techniques*, *13*(11), 6175–6191. <https://doi.org/10.5194/amt-13-6175-2020>
- Liu, S., Valks, P., Pinardi, G., De Smedt, I., Yu, H., Beirle, S., & Richter, A. (2019). An improved total and tropospheric NO₂ column retrieval for GOME-2. *Atmospheric Measurement Techniques*, *12*(2), 1029–1057. <https://doi.org/10.5194/amt-12-1029-2019>
- Liu, S., Valks, P., Pinardi, G., Xu, J., Chan, K. L., Argyrouli, A., et al. (2021). An improved TROPOMI tropospheric NO₂ research product over Europe. *Atmospheric Measurement Techniques*, *14*(11), 7297–7327. <https://doi.org/10.5194/amt-14-7297-2021>
- Lorente, A., Folkert Boersma, K., Yu, H., Dörner, S., Hilboll, A., Richter, A., et al. (2017). Structural uncertainty in air mass factor calculation for NO₂ and HCHO satellite retrievals. *Atmospheric Measurement Techniques*, *10*(3), 759–782. <https://doi.org/10.5194/amt-10-759-2017>
- Nakoudi, K., Giannakaki, E., Dandou, A., Tombrou, M., & Komppula, M. (2019). Planetary boundary layer height by means of lidar and numerical simulations over New Delhi, India. *Atmospheric Measurement Techniques*, *12*(5), 2595–2610. <https://doi.org/10.5194/amt-12-2595-2019>
- Pinardi, G., Van Roozendaal, M., Hendrick, F., Theys, N., Abuhassan, N., Bais, A., et al. (2020). Validation of tropospheric NO₂ column measurements of GOME-2A and OMI using MAX-DOAS and direct sun network observations. *Atmospheric Measurement Techniques*, *13*(11), 6141–6174. <https://doi.org/10.5194/amt-13-6141-2020>
- Qu, Z., Henze, D. K., Worden, H. M., Jiang, Z., Gaubert, B., Theys, N., & Wang, W. (2022). Sector-based top-down estimates of NO_x, SO₂, and CO emissions in East Asia. *Geophysical Research Letters*, *49*(2), e2021GL096009. <https://doi.org/10.1029/2021gl096009>
- Sharma, A., Ojha, N., Pozzer, A., Mar, K. A., Beig, G., Lelieveld, J., & Gunthe, S. S. (2017). WRF-chem simulated surface ozone over south Asia during the pre-monsoon: Effects of emission inventories and chemical mechanisms. *Atmospheric Chemistry and Physics*, *17*(23), 14393–14413. <https://doi.org/10.5194/acp-17-14393-2017>
- Shu, L., Zhu, L., Bak, J., Zoogman, P., Han, H., Long, X., et al. (2022). Improved ozone simulation in East Asia via assimilating observations from the first geostationary air-quality monitoring satellite: Insights from an Observing System Simulation Experiment. *Atmospheric Environment*, *274*, 119003. <https://doi.org/10.1016/j.atmosenv.2022.119003>
- Sicard, P., Crippa, P., De Marco, A., Castruccio, S., Giani, P., Cuesta, J., et al. (2021). High spatial resolution WRF-chem model over Asia: Physics and chemistry evaluation. *Atmospheric Environment*, *244*, 118004. <https://doi.org/10.1016/j.atmosenv.2020.118004>
- Su, T., Li, J., Li, C., Xiang, P., Lau, A. K.-H., Guo, J., et al. (2017). An intercomparison of long-term planetary boundary layer heights retrieved from CALIPSO, ground-based lidar, and radiosonde measurements over Hong Kong. *Journal of Geophysical Research: Atmospheres*, *122*(7), 3929–3943. <https://doi.org/10.1002/2016jd025937>
- Theys, N., De Smedt, I., Yu, H., Lerot, C., & Van Roozendaal, M. (2022). TROPOMI SO₂ ATBD (Tech. Rep.). S5P-BIRA-L2-ATBD-400E issue 2.3.1.
- van Geffen, J., Boersma, K. F., Eskes, H., Sneep, M., Ter Linden, M., Zara, M., & Veefkind, J. P. (2020). S5P TROPOMI NO₂ slant column retrieval: Method, stability, uncertainties and comparisons with OMI. *Atmospheric Measurement Techniques*, *13*(3), 1315–1335. <https://doi.org/10.5194/amt-13-1315-2020>

- Verhoelst, T., Compernelle, S., Pinardi, G., Lambert, J.-C., Eskes, H. J., Eichmann, K.-U., et al. (2021). Ground-based validation of the Copernicus Sentinel-5p TROPOMI NO₂ measurements with the NDACC ZSL-DOAS, MAX-DOAS and Pandonia global networks. *Atmospheric Measurement Techniques*, *14*(1), 481–510. <https://doi.org/10.5194/amt-14-481-2021>
- Wang, C., Wang, T., Wang, P., & Raktin, V. (2020). Comparison and validation of TROPOMI and OMI NO₂ observations over China. *Atmosphere*, *11*(6), 636. <https://doi.org/10.3390/atmos11060636>
- Wang, C., Wang, T., Wang, P., & Wang, W. (2022). Assessment of the performance of TROPOMI NO₂ and SO₂ data products in the North China Plain: Comparison, correction and application. *Remote Sensing*, *14*(1), 214. <https://doi.org/10.3390/rs14010214>